A nonlinear disturbance observer-based adaptive integral sliding mode control for missile guidance system

Handan Gürsoy-Demir & Mehmet Önder Efe

Taylor & Francis
Taylor & Francis Group

Check for updates

A nonlinear disturbance observer-based adaptive integral sliding mode control for missile guidance system

Handan Gürsoy-Demir [a,b] and Mehmet Önder Efe [c]

aGraduate School of Science and Engineering, Hacettepe University, Ankara, Turkey; bDepartment of Computer Engineering, Iskenderun Technical University, Hatay, Turkey; cDepartment of Computer Engineering, Hacettepe University, Ankara, Turkey

ABSTRACT

A novel composite three-dimensional (3D) guidance law based on an adaptive integral sliding mode (AISM) control utilizing a nonlinear disturbance observer (NDOB) technique is proposed for missiles. First, an integral sliding mode control is selected as the guidance law to get rid of the reaching phase of sliding mode control. Second, the switching gains are adjusted by designing an adaptive law. Finally, the NDOB is designed to estimate and compensate for the unknown target accelerations that are considered as the disturbance. Thus the NDOB and AISM law are combined into a novel composite guidance law to improve performance and to reduce the chattering phenomenon. Finally, to verify the effectiveness and robustness, numerical simulations are performed in different scenarios and these results are presented comparatively with the augmented proportional navigation (APN) and the AISM guidance law. Moreover, the proposed law outperforms the other schemes regarding the miss distance and interception time.

1. Introduction

Guidance law design, which is used to determine the appropriate acceleration commands that will reduce the distance to the target to zero or to an acceptably small value in a finite time, has continued to attract the attention of many researchers. Proportional navigation (PN) guidance law is commonly used by many scholars and engineers due to its high performance and simplicity of implementation (Murtaugh and Criel 1966; Dhananjay, Lum, and Xu 2012). In addition, its variants, which are ideal proportional navigation (IPN), pure proportional navigation (PPN), augmented proportional navigation (APN), true proportional navigation (TPN) etc., are proposed to display better performance. However, PN guidance and its variants may not perform sufficiently well against the target with high maneuverability and they may introduce some disadvantages, such as a large miss distance and overload saturation. In recent years, different guidance methods have been proposed for nonlinear control methods, such as $\mathcal{H}_\infty$ guidance (Yaghi and Efe 2020), finite-time

---

CONTACT Handan Gürsoy-Demir ✉ handangrsy@gmail.com

guidance (Zhang et al. 2016), sliding mode guidance (Harl and Balakrishnan 2011; Hu, Han, and Xin 2019), etc.

Sliding mode control (SMC) is an effective and robust nonlinear control method because of the ability to eliminate matched external disturbances and parameter uncertainties (Utkin 1977). Up to now, this method has been used for a wide range of scientific and industrial problems, such as robotics (Jia et al. 2019), electro-mechanical systems (Utkin, Guldner, and Shi 2009; Wang et al. 2020), stochastic Markovian jumping systems (Chen, Jia, and Niu 2016) and so on. Despite its prominent features, there are two major problems when using SMC. These problems are the emergence of reaching phase, which causes unnecessarily large control signals, and the chattering phenomenon. Researchers have proposed various SMC strategies to overcome these deficiencies and to improve the performance of control. Moreover, several researchers have used traditional SMCs together with other control algorithms. Some of these methods are high-order SMC, terminal SMC, integral SMC, fuzzy SMC (Mehmet Önder 2011; Chen et al. 2019; Hou et al. 2016; Chen et al. 2020).

The integral sliding mode control method (Utkin and Shi 1996) is one of the sophisticated SMC methods and its literature that addressed both linear and nonlinear systems in a variety of control fields has been growing rapidly (Nair, Behera, and Kumar 2017; Wang et al. 2019). This method intends to eliminate the reaching phase to ensure the invariance of the SMC from the initial instant of time according to the traditional SMC method. Thus the system can guarantee robustness throughout the entire response. However, there is a significant shortcoming concerning the ISMC method. Determining the switching gain is always a troublesome process, such that the upper bound of the external disturbance needs to be known and this gain should be chosen larger than this upper bound. Most of the research outcomes on the ISMC method are based on assumptions about the upper bound disturbance knowledge. However, this is not always possible in practical applications. To overcome the above-mentioned problem, the adaptive law is proposed in the previous studies and this has enabled the development of an adaptive integral sliding mode control (Li et al. 2019; Song and Song 2016).

The chattering phenomenon is the major disadvantage in the use of the SMC and its proposed variants. This problem, referred to as high-frequency oscillations in the control signal, results in unnecessary wear and tear of the actuator. To date, various techniques have been used to remedy the chattering phenomenon, such as the saturation function, the boundary layer, the high order SMC and so on. To overcome this phenomenon, the above-listed methods need the upper bound of the disturbance as well. Therefore, a new scheme called the disturbance observer-based control is designed. The disturbance observer (DOB) is an efficient technique to observe parameter uncertainties and external disturbances in the system (Sariyildiz, Oboe, and Ohnishi 2019; Luo et al. 2021). Although this technique appears in different names and prospects in terms of design, all of them have the same idea, which estimates the disturbance or uncertainties of the system and then compensates by making use of the estimate. This technique has been applied in many different fields in the literature since it was designed by Ohishi (1983).

In practice, the missile and the target relative motion that occurs in three-dimensional geometry are described by the mathematical model consisting of second-order nonlinear strongly coupled differential equations. In the three dimensions, the missile and the target's relative motion can be decoupled into two planar relative movements and these movements

are designed by ignoring the cross-couplings between the elevation and the azimuth. Thus far, there are many researchers who have constructed guidance laws in 2D geometry as such simplifications make it much easier to design and analyze guidance laws. During these simplifications, however, some guidance information can be lost, and this is an undesirable situation as it can lead to poor results about guidance accuracy.

Golestani et al. (2015) proposed a finite-time integral sliding mode scheme for the missile guidance system regarding the geometry of planar interception. In Li et al. (2019), an adaptive ISM guidance law was presented for planar engagement geometry with respect to impact angle constraint considering autopilot lag. A sliding surface, which was acceleration, the LOS angular rate and LOS angle tracking error were considered together, was designed in that paper. In the study of Zhang et al. (2019), impact angle control over guidance based on ISM manifold with finite-time control was proposed and also the second-order extended state observer (ESO) was used. Besides, the missile and target were designed with a point mass model. In Zhang, Li, and Luo (2013a), a composite guidance law based on an ISM method and NDOB technique is proposed for missile intercepting maneuvering targets in the geometry of the planar interception. Liang et al. (2014) proposed a robust guidance law by utilizing an ISM scheme and both the missile and the target were taken to be a point-mass model. Meng and Zhou (2018) presented a new guidance law by using a super-twisting algorithm with nonlinear ISM by considering missile autopilot dynamics for planar missile-target engagement. Besides, the finite time disturbance observer was utilized herein to handle the disturbances resulting from the acceleration of the target. Zhang, Li, and Luo (2013) designed the terminal guidance law by using both the linear and nonlinear ISM control methods and the NDOB technique by considering impact angle constraints. In addition, point-mass model was used in the missile and target design in that paper. Song and Song (2016) proposed the guidance law in three-dimensional space by using the ISMC. Then, an adaptive guidance law based on ISMC improved to estimate the target acceleration's upper bound. Wang and He (2016) proposed a guidance law for intercepting targets that are maneuvering with LOS angle constraints. They used an optimal SMC guidance law and developed the equivalent control part of the SMC method using the model predictive control to satisfy terminal angle constraint in that paper. Moreover, the missile and target were taken to be a point-mass and this law was designed for planar missile–target engagement.

The guidance laws designed so far and based on the ISM method in the literature have been examined and presented above. In this paper, the novel composite guidance law based on the AISM control technique as well as the NDOB is proposed for three dimensional engagement geometry and the main contributions of this study are threefold. First, the AISM guidance law is developed by being considered three-dimensional missile-target interception geometry. Thus the reaching phase of the sliding mode is eliminated and also the designed guidance law has made it possible for the system response to be robust from the very beginning. Second, the adaptive law is designed to tune the switching gain and so the upper bound information of the target accelerations does not need to be known. In addition, this law guarantees the LOS angular rates converge to zero in finite time. Third, motivated by the work of Zhang et al. (2016), the NDOB technique is presented to estimate and compensate the target acceleration, which is tackled as the disturbance without the upper bound information. Thanks to the NDOB technique, the chattering phenomenon, which is the major problem of the SMC method, is alleviated. Thus a novel guidance law

consisting of a combination of the AISM guidance law and the NDOB technique is presented. Finally, in missile guidance systems, it is very important to overcome the deviations in the LOS angles and to be able to create high guidance accuracy under the influence of noise and uncertainties. In this case, a novel composite guidance law was designed in the simulation environment, and the efficacy and robustness of the new proposed guidance law are investigated using a 6-DOF nonlinear model via simulation studies.

The rest of this paper is structured as follows. Missile-target engagement geometry is formulated in Section 2. In Section 3, the design procedure of the proposed composite guidance law is presented comprehensively. In Section 4, numerical simulations and their results are presented to verify the effectiveness of the proposed guidance law and the concluding remarks are constituted in Section 5.

2. Missile-target engagement geometry

In this section, the missile-target relative motion in three-dimensional environment is briefly explained and is presented in Figure 1.

In Figure 1, T and M denote the target and the missile, respectively. R is the range between the missile and target. θ and ϕ are the elevation angle and the azimuth angle of the line-of-sight. The second-order nonlinear differential equations of engagement geometry in Guo, Li, and Zhou (2019) can be given as

$$\ddot{R} - R\dot{\phi}^2 - R\dot{\theta}^2 \cos^2 \phi = a_{TR} - a_{MR} \tag{1}$$

$$R\ddot{\phi} + 2\dot{R}\dot{\phi} + R\dot{\theta}^2 \sin \phi \cos \phi = a_{T\phi} - a_{M\phi} \tag{2}$$

$$R\ddot{\theta} \cos \phi + 2\dot{R}\dot{\theta} \cos \phi - 2R\dot{\phi}\dot{\theta} \sin \phi = a_{M\theta} - a_{T\theta} \tag{3}$$

where $a_{TR}, a_{T\theta}, a_{T\phi}$ are the accelerations of target and $a_{MR}, a_{M\theta}, a_{M\phi}$ are the accelerations of missile in the LOS frame. One of the main objectives of the guidance laws is to obtain
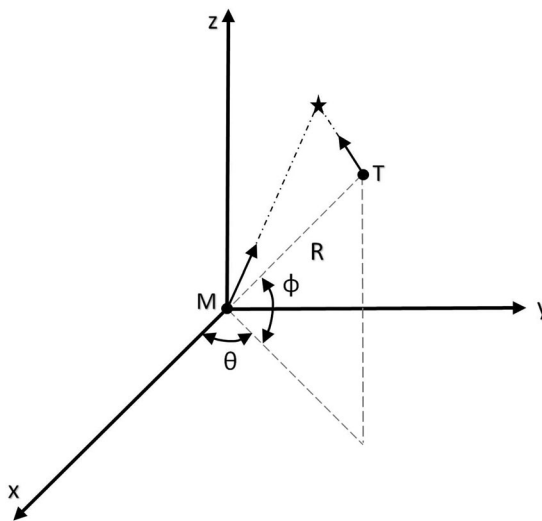

Figure 1. Missile-target engagement geometry.

zero LOS angular rates, $\dot{\theta}$ and $\dot{\phi}$. Equations (4) and (5) are used in the design of the guidance laws.

$$\ddot{\phi} = -\frac{2\dot{R}}{R}\dot{\phi} - \dot{\theta}^2 \sin\phi\cos\phi - \frac{a_{M\phi}}{R} + \frac{a_{T\phi}}{R} \tag{4}$$

$$\ddot{\theta} = -\frac{2\dot{R}}{R}\dot{\theta} + 2\dot{\theta}\dot{\phi}\tan\phi + \frac{a_{M\theta}}{R\cos\phi} - \frac{a_{T\theta}}{R\cos\phi} \tag{5}$$

3. Guidance law design

3.1. Preliminaries

Lemma 3.1 (Yu et al. 2005): *Let k_i for $(i = 1, 2, \ldots, n)$ are all positive numbers. Following inequality is satisfied for $0 < q < 2$.*

$$\left(k_1^2 + k_2^2 + \cdots + k_n^2\right)^q \leq \left(k_1^q + k_2^q + \cdots + k_n^q\right)^2 \tag{6}$$

Lemma 3.2 (Yu et al. 2005): *Let $V(t)$ be a continuous positive definite Lyapunov function as well as t_0 is the initial time. If $\dot{V}(t) \leq -\kappa_1 V(t) - \kappa_2 V(t)^\xi$ $(\forall t > t_0)$, where $\kappa_1, \kappa_2 > 0$, $0 < \xi < 1$. Then, $V(t)$ converges to the equilibrium point in finite time if given by*

$$t_f \leqslant t_0 + \frac{1}{\kappa_1(1-\xi)}\ln\left(\frac{\kappa_1 V(t_0)^{1-\xi} + \kappa_2}{\kappa_2}\right) \tag{7}$$

Lemma 3.3 (Bhat and Bernstein 2005): *A necessary condition for a polynomial $D(x) = x^n + a_n x^{n-1} + \cdots + a_2 x + a_1$ of a complex variable x to be Hurwitz is $a_1, a_2, \ldots .a_n > 0$.*
For an nth-order system with input u,

$$\dot{y}_1 = y_2, \quad \dot{y}_2 = y_3, \ldots, \dot{y}_{n-1} = y_n, \quad \dot{y}_n = u \tag{8}$$

there exists an $\varepsilon \in (0, 1)$ such that, for every $\alpha \in (1 - \varepsilon, 1)$ the equilibrium at origin is reached in finite time under the following feedback law for the system given in (8).

$$u = -a_1\operatorname{sgn}(y_1)\left|y_1\right|^{\alpha_1} - \cdots - a_n\operatorname{sgn}(y_n)\left|y_n\right|^{\alpha_n} \tag{9}$$

where $\alpha_1, \alpha_2, \ldots, \alpha_n$ satisfy $\alpha_{i-1} = \frac{\alpha_i \alpha_{i+1}}{2\alpha_{i+1} - \alpha_i}$ $(i = 2, \ldots, n)$, $\alpha_n = \alpha$, $\alpha_{n+1} = 1$.

Lemma 3.4 (Khalil 2002; Man, Zhang, and Li 2019): *(Input-to-State Stability Theorem, ISS Theorem) Consider the nonlinear system of the following form:*

$$\dot{x}(t) = f(x, u, t) \tag{10}$$

If the system $\dot{x} = f(x, 0, t)$ is globally asymptotically stable and also $\lim_{t\to\infty} u = 0$, this system's states converge asymptotically to zero, i.e. $\lim_{t\to\infty} x = 0$.

Assumption 3.1 (Li et al. 2019): *It is assumed that the target accelerations $|a_{T\phi}| \leq \epsilon_1$ and $|a_{T\theta}| \leq \epsilon_2$, where ϵ_1 and ϵ_2 are two positive yet unknown constants.*

3.2. Adaptive integral sliding mode approach for guidance law design

The nonlinear ISM guidance law is showed to intercept a target in three-dimensional engagement geometry under the external disturbances in this section. However, this guidance law needs the upper bound of the acceleration of the target. Therefore, the adaptive law is designed to estimate the upper bound of the target's accelerations denoted by ϵ_1 and ϵ_2. The stability of the given system is proven by using the Lyapunov's stability theorem. The system dynamics in (4)–(5) can be rewritten as follows:

$$x_1 = \phi, \quad x_2 = \dot{\phi}, \quad x_3 = \theta, \quad x_4 = \dot{\theta}$$
$$\dot{x}_1 = x_2$$
$$\dot{x}_2 = -\frac{2\dot{R}}{R}x_2 - x_4^2 \sin x_1 \cos x_1 - \frac{a_{M\phi}}{R} + \frac{a_{T\phi}}{R} \tag{11}$$
$$\dot{x}_3 = x_4$$
$$\dot{x}_4 = -\frac{2\dot{R}}{R}x_4 + 2x_4 x_2 \tan x_1 + \frac{a_{M\theta}}{R\cos x_1} - \frac{a_{T\theta}}{R\cos x_1} \tag{12}$$

For the nonlinear ISM guidance law, a sliding manifold vector is described (Zhang, Li, and Luo 2013a; Song and Song 2016) as follows:

$$s = \begin{pmatrix} s_1 \\ s_2 \end{pmatrix} = \begin{pmatrix} x_2 - x_2(t_0) + \int_0^t (a_1 \mathrm{sgn}(x_1) |x_1|^{\alpha_1} + a_2 \mathrm{sgn}(x_2) |x_2|^{\alpha_2})\, dt \\ x_4 - x_4(t_0) + \int_0^t (b_1 \mathrm{sgn}(x_3) |x_3|^{\beta_1} + b_2 \mathrm{sgn}(x_4) |x_4|^{\beta_2})\, dt \end{pmatrix} \tag{13}$$

where $a_1, a_2, b_1, b_2 > 0, 0 < \alpha_1 < 1, 0 < \beta_1 < 1, \alpha_2 = \frac{2\alpha_1}{\alpha_1+1}, \beta_2 = \frac{2\beta_1}{\beta_1+1}$ are the parameters to be designed. In addition, $a_1, a_2, b_1, b_2 > 0$ ensure that the two polynomials $\lambda^2 + a_2\lambda + a_1$ and $\lambda^2 + b_2\lambda + b_1$ are Hurwitz. Besides, it should be known that sliding mode starts from the initial time instance since $s_1(t_0) = 0, s_2(t_0) = 0$ at $t = t_0$.

The time derivative of the sliding surfaces given in (13) is obtained as below.

$$\dot{s} = \begin{pmatrix} \dot{s}_1 \\ \dot{s}_2 \end{pmatrix} = \begin{pmatrix} \dot{x}_2 + (a_1 \mathrm{sgn}(x_1) |x_1|^{\alpha_1} + a_2 \mathrm{sgn}(x_2) |x_2|^{\alpha_2}) \\ \dot{x}_4 + (b_1 \mathrm{sgn}(x_3) |x_3|^{\beta_1} + b_2 \mathrm{sgn}(x_4) |x_4|^{\beta_2}) \end{pmatrix} \tag{14}$$

Substituting $\dot{x}_2$ and $\dot{x}_4$ given in (11)–(12) into (14), the following derivative is obtained

$$\dot{s} = \begin{pmatrix} \dot{s}_1 \\ \dot{s}_2 \end{pmatrix} = \begin{pmatrix} -\dfrac{2\dot{R}}{R}x_2 - x_4^2 \sin x_1 \cos x_1 - \dfrac{a_{M\phi}}{R} + \dfrac{a_{T\phi}}{R} \\ +(a_1 \mathrm{sgn}(x_1) |x_1|^{\alpha_1} + a_2 \mathrm{sgn}(x_2) |x_2|^{\alpha_2}) \\ -\dfrac{2\dot{R}}{R}x_4 + 2x_4 x_2 \tan x_1 + \dfrac{a_{M\theta}}{R\cos x_1} - \dfrac{a_{T\theta}}{R\cos x_1} \\ +(b_1 \mathrm{sgn}(x_3) |x_3|^{\beta_1} + b_2 \mathrm{sgn}(x_4) |x_4|^{\beta_2}) \end{pmatrix}. \tag{15}$$

Equation (15) can be rewritten as given by (16).

$$\dot{s} = A + B \begin{pmatrix} a_{M\phi} \\ a_{M\theta} \end{pmatrix} + C \begin{pmatrix} a_{T\phi} \\ a_{T\theta} \end{pmatrix} \tag{16}$$

where

$$A = \begin{pmatrix} -\dfrac{2\dot{R}}{R}x_2 - x_4^2 \sin x_1 \cos x_1 + (a_1\text{sgn}(x_1)\,|x_1|^{\alpha_1} \\ \qquad\qquad + a_2\text{sgn}(x_2)\,|x_2|^{\alpha_2}) \\ -\dfrac{2\dot{R}}{R}x_4 + 2x_4 x_2 \tan x_1 + (b_1\text{sgn}(x_3)\,|x_3|^{\beta_1} \\ \qquad\qquad + b_2\text{sgn}(x_4)\,|x_4|^{\beta_2}) \end{pmatrix}$$

$$B = \begin{pmatrix} -\dfrac{1}{R} & 0 \\ 0 & \dfrac{1}{R\cos x_1} \end{pmatrix} \quad C = \begin{pmatrix} \dfrac{1}{R} & 0 \\ 0 & -\dfrac{1}{R\cos x_1} \end{pmatrix}.$$

In the guidance system based on ISM, upper bounds of the target accelerations need to be known numerically. According to Assumption 3.1, in a practical operation scenario, it is not possible to obtain knowledge of the upper bound of the target accelerations a priori. Thus an adaptive law and the AISM guidance law are designed as defined in Song and Song (2016). In the presented guidance law, the adaptive law aims to estimate the upper bound for the target accelerations.

Theorem 3.1: *Let* (11) *and* (12) *denote the system dynamics and let* (17) *be the chosen control law.*

$$\begin{pmatrix} a_{M\phi} \\ a_{M\theta} \end{pmatrix} = B^{-1}\left(-A - \rho_1 s - \rho_2 \begin{pmatrix} |s_1|^{\gamma}\,\text{sgn}(s_1) \\ |s_2|^{\gamma}\,\text{sgn}(s_2) \end{pmatrix} - \sum_{j=1}^{2}\left(\begin{vmatrix} c_{1j} \\ c_{2j} \end{vmatrix}\begin{matrix} \text{sgn}(s_1) \\ \text{sgn}(s_2) \end{matrix} \right)\eta_j\widehat{\epsilon}_j \right) \quad (17)$$

where $\rho_1, \rho_2 > 0,\ 0 < \gamma < 1,\ \eta_1, \eta_2 > 1$ *and* $\widehat{\epsilon}_j$ *is an adaptive estimate of* ϵ_j *(j = 1, 2).*
  Define the estimation error as $\tilde{\epsilon}_j := \epsilon_j - \widehat{\epsilon}_j$ *and the adaptive law for* $\widehat{\epsilon}_j$ *as follows:*

$$\dot{\widehat{\epsilon}}_j = \eta_j\left(\sum_{i=1}^{2}|c_{ij}|\,|s_i| \right), \quad \widehat{\epsilon}_j(0) > 0, \quad j = 1, 2 \quad (18)$$

Under these conditions $\dot{\theta}$ *and* $\dot{\phi}$*, which are the LOS angular rates, will converge to zero in finite time.*

Proof: This guidance law can be studied in three steps. These steps are given below.
  Step 1: The switching variables given in (13) and estimation errors $\tilde{\epsilon}_j$ are bounded.
  Step 2: The switching variables given in (13) converge to zero in finite time.
  Step 3: The states x_2 and x_4 given in (11) and (12) converge to zero in finite time.
  Step 1: Choose the Lyapunov function candidate as follows:

$$V_1 = \frac{1}{2}s^T s + \frac{1}{2}\sum_{j=1}^{2}\tilde{\epsilon}_j^2 \quad (19)$$

The time derivative of V_1 is obtained as given below:

$$\dot{V}_1 = s^T \dot{s} + \sum_{j=1}^{2}\tilde{\epsilon}_j\dot{\tilde{\epsilon}}_j \quad (20)$$

Equation (20) along the guidance system in (17) and the adaptive law in (18) is

$$\dot{V}_1 = s^T \dot{s} + \sum_{j=1}^{2} \tilde{\epsilon}_j \dot{\tilde{\epsilon}}_j$$

$$= s^T \left(A + B \begin{pmatrix} a_{M\phi} \\ a_{M\theta} \end{pmatrix} + C \begin{pmatrix} a_{T\phi} \\ a_{T\theta} \end{pmatrix} \right) + \sum_{j=1}^{2} \tilde{\epsilon}_j \dot{\tilde{\epsilon}}_j$$

$$= s^T \left(-\rho_1 s - \rho_2 \begin{pmatrix} |s_1|^{\gamma} \operatorname{sgn}(s_1) \\ |s_2|^{\gamma} \operatorname{sgn}(s_2) \end{pmatrix} - \sum_{j=1}^{2} \begin{pmatrix} |c_{1j}|\operatorname{sgn}(s_1) \\ |c_{2j}|\operatorname{sgn}(s_2) \end{pmatrix} \eta_j \widehat{\epsilon}_j + C \begin{pmatrix} a_{T\phi} \\ a_{T\theta} \end{pmatrix} \right) + \sum_{j=1}^{2} \tilde{\epsilon}_j \dot{\tilde{\epsilon}}_j$$

$$= \left(-\rho_1 s^T s - \rho_2 \sum_{i=1}^{2} |s_i|^{\gamma+1} - \sum_{j=1}^{2} \left(\sum_{i=1}^{2} |c_{ij}||s_i| \right) \eta_j \widehat{\epsilon}_j \right) + \left(\sum_{i=1}^{2} c_{i1} s_i \right) a_{T\phi} + \left(\sum_{i=1}^{2} c_{i2} s_i \right) a_{T\theta}$$

$$- \sum_{j=1}^{2} \left(\sum_{i=1}^{2} |c_{ij}||s_i| \right) \eta_j (\epsilon_j - \widehat{\epsilon}_j)$$

$$= -\rho_1 s^T s - \rho_2 \sum_{i=1}^{2} |s_i|^{\gamma+1} + \left(\sum_{i=1}^{2} c_{i1} s_i \right) a_{T\phi} + \left(\sum_{i=1}^{2} c_{i2} s_i \right) a_{T\theta} - \sum_{j=1}^{2} \left(\sum_{i=1}^{2} |c_{ij}||s_i| \right) \eta_j \epsilon_j$$

$$\leqslant -\rho_1 s^T s - \rho_2 \sum_{i=1}^{2} |s_i|^{\gamma+1} + \sum_{j=1}^{2} \left(\sum_{i=1}^{2} |c_{ij}||s_i| \right) \epsilon_j - \sum_{j=1}^{2} \left(\sum_{i=1}^{2} |c_{ij}||s_i| \right) \eta_j \epsilon_j$$

$$= -\rho_1 s^T s - \rho_2 \sum_{i=1}^{2} |s_i|^{\gamma+1} + \sum_{j=1}^{2} \left(\sum_{i=1}^{2} |c_{ij}||s_i| \right) \epsilon_j (1 - \eta_j)$$

$$\leqslant -\rho_1 s^T s - \rho_2 \sum_{i=1}^{2} |s_i|^{\gamma+1} \tag{21}$$

According to (21), for $V_1 > 0$, $\dot{V}_1 \leqslant 0$ is obtained and s and $\tilde{\epsilon}_j (j = 1, 2)$ are bounded. This completes the claim in the first step.

Step 2. The Lyapunov function is selected as $V_2 = \frac{1}{2} s^T s$ and the derivative of this Lyapunov function as follows:

$$\dot{V}_2 = s^T \dot{s} = s^T \left(A + B \begin{pmatrix} a_{M\phi} \\ a_{M\theta} \end{pmatrix} + C \begin{pmatrix} a_{T\phi} \\ a_{T\theta} \end{pmatrix} \right)$$

$$= s^T \left(-\rho_1 s - \rho_2 \begin{pmatrix} |s_1|^{\gamma} \operatorname{sgn}(s_1) \\ |s_2|^{\gamma} \operatorname{sgn}(s_2) \end{pmatrix} - \sum_{j=1}^{2} \begin{pmatrix} |c_{1j}|\operatorname{sgn}(s_1) \\ |c_{2j}|\operatorname{sgn}(s_2) \end{pmatrix} \eta_j \widehat{\epsilon}_j + C \begin{pmatrix} a_{T\phi} \\ a_{T\theta} \end{pmatrix} \right)$$

$$\leqslant -\rho_1 s^T s - \rho_2 \sum_{i=1}^{2} |s_i|^{\gamma+1} - \sum_{j=1}^{2} \left(\sum_{i=1}^{2} |c_{ij}||s_i| \right) \eta_j \widehat{\epsilon}_j$$

$$+ \sum_{j=1}^{2} \left(\sum_{i=1}^{2} |c_{ij}||s_i| \right) \epsilon_j$$

$$= -\rho_1 s^T s - \rho_2 \sum_{i=1}^{2} |s_i|^{\gamma+1} + \sum_{j=1}^{2} \left(\sum_{i=1}^{2} |c_{ij}||s_i| \right) (\epsilon_j - \eta_j \widehat{\epsilon_j}) \tag{22}$$

Since $\widehat{\epsilon}_j(0) > 0$ and $\dot{\widehat{\epsilon}}_j \geq 0$, we have $\widehat{\epsilon}_j(t) \geq \widehat{\epsilon}_j(0) \geq 0$. If $\widehat{\epsilon}_j(0)$ is large enough, i.e. $\widehat{\epsilon}_j(0) > |\widetilde{\epsilon}_j(0)|$, η_j satisfies the following inequality as given in Song, Song, and Zhou (2016); Si and Song (2019).

$$\eta_j \geq 1 + \frac{\sqrt{\widehat{\epsilon}_j^2(0) + s_j^2(0)}}{\widehat{\epsilon}_j(0)}, \quad j = 1,2 \tag{23}$$

Accordingly, the following inequalities can be written by considering $\widehat{\epsilon}_j(t) \geq \widehat{\epsilon}_j(0) \geq 0$.

$$\epsilon_j(0) - \eta_j \widehat{\epsilon}_j(0) \leq \epsilon_j(0) - \widehat{\epsilon}_j(0) - \sqrt{\widehat{\epsilon}_j^2(0) + s_j^2(0)}$$

$$\leq \widetilde{\epsilon}_j(0) - \sqrt{\widehat{\epsilon}_j^2(0) + s_j^2(0)}$$

$$\leq |\widetilde{\epsilon}_j(0)| - \sqrt{\widehat{\epsilon}_j^2(0) + s_j^2(0)}$$

$$\leq \sqrt{\widetilde{\epsilon}_j^2(0)} - \sqrt{\widehat{\epsilon}_j^2(0) + s_j^2(0)}$$

$$\leq \sqrt{\widehat{\epsilon}_j^2(0)} - \sqrt{\widehat{\epsilon}_j^2(0) + s_j^2(0)}$$

$$\leq 0 \tag{24}$$

Based on Lemma 3.1, Equation (25), given below, is obtained by using (22) and (24).

$$\dot{V}_2 \leq -\rho_1 s^T s - \rho_2 \sum_{i=1}^{2} |s_i|^{\gamma+1}$$

$$\leq -2\rho_1 V_2 - 2^{\frac{\gamma+1}{2}} \rho_2 V_2^{\frac{\gamma+1}{2}} \tag{25}$$

The final inequality above stipulates that the switching variables converge to zero in finite time according to Lemma 3.2. This completes the claim in the second step.

Step 3: Finally, the states x_2 and x_4 given in (11) and (12) are studied. It is clearly known that $s_1 = 0$ and $s_2 = 0$, $\dot{s}_1 = 0$ and $\dot{s}_2 = 0$ on the sliding surface. In (15), if $\dot{x}_2$ and $\dot{x}_4$ are separated, the following equations are obtained:

$$\dot{x}_2 = -(a_1 \text{sgn}(x_1) |x_1|^{\alpha_1} + b_1 \text{sgn}(x_2) |x_2|^{\alpha_2}) \tag{26}$$

$$\dot{x}_4 = -(a_1 \text{sgn}(x_3) |x_3|^{\beta_1} + b_1 \text{sgn}(x_4) |x_4|^{\beta_2}) \tag{27}$$

According to Lemma 3.3, in the closed loop, the states x_2 and x_4 converge to zero in finite time, that is, the LOS angular rates $\dot{\theta}$ and $\dot{\phi}$ will converge to zero in finite time as a result of the chosen guidance strategy. ∎

4. Composite guidance law design

4.1. Design of nonlinear disturbance observer

Assumption 4.1 (Zhang et al. 2016; Man, Liu, and Li 2019): *We assume that the final values of the time derivative of target accelerations $\dot{a}_{T\theta}$ and $\dot{a}_{T\phi}$ are zero, i.e. $\lim_{t\to\infty} \dot{a}_{T\theta} = 0$ and $\lim_{t\to\infty} \dot{a}_{T\phi} = 0$.*

The guidance system in (4)–(5) can be rewritten as follows:

$$\dot{x}_2 = A_1 + B_1 \left(a_{M\phi} - a_{T\phi}\right) \tag{28}$$

$$\dot{x}_4 = A_2 + B_2 \left(a_{M\theta} - a_{T\theta}\right) \tag{29}$$

where

$$A = \begin{pmatrix} A_1 \\ A_2 \end{pmatrix} = \begin{pmatrix} -\dfrac{2\dot{R}}{R}x_2 - x_4^2 \sin x_1 \cos x_1 \\[2ex] -\dfrac{2\dot{R}}{R}x_4 + 2x_4 x_2 \tan x_1 \end{pmatrix} \qquad B = \begin{pmatrix} B_1 \\ B_2 \end{pmatrix} = \begin{pmatrix} -\dfrac{1}{R} \\[2ex] \dfrac{1}{R\cos x_1} \end{pmatrix}.$$

Theorem 4.1 (Zhang et al. 2016): *Let Assumption 3.1 holds true and let the NDOB dynamics is given by the following equations. The predicted target accelerations asymptotically converge to the target accelerations if $z_1(0) = x_2(0)$ and $z_2(0) = x_4(0)$ hold true.*

$$\begin{aligned} \dot{z}_1 &= A_1 + B_1 \left(a_{M\phi} - \widehat{a}_{T\phi}\right) \\ \widehat{a}_{T\phi} &= \omega_1 \left(x_2 - z_1\right) \end{aligned} \tag{30}$$

$$\begin{aligned} \dot{z}_2 &= A_2 + B_2 \left(a_{M\theta} - \widehat{a}_{T\theta}\right) \\ \widehat{a}_{T\theta} &= \omega_2 \left(x_4 - z_2\right) \end{aligned} \tag{31}$$

where $\omega_1 > 0$ and $\omega_2 < 0$.

Proof: Let $e_{T\phi}$ and $e_{T\theta}$ be the disturbance prediction errors and are expressed as $e_{T\phi} := a_{T\phi} - \widehat{a}_{T\phi}$ and $e_{T\theta} := a_{T\theta} - \widehat{a}_{T\theta}$. Then, their behaviors are obtained using (28)–(31) as follows:

$$\begin{aligned} \dot{e}_{T\phi} &= \dot{a}_{T\phi} - \omega_1 \left(\dot{x}_2 - \dot{z}_1\right) \\ &= \dot{a}_{T\phi} - \omega_1 \big((A_1 + B_1(a_{M\phi} - a_{T\phi}) \\ &\quad - A_1 - B_1 \left(a_{M\phi} - \widehat{a}_{T\phi}\right)\big) \\ &= \dot{a}_{T\phi} + \omega_1 B_1 \left(a_{T\phi} - \widehat{a}_{T\phi}\right) \\ &= \dot{a}_{T\phi} + \omega_1 B_1 e_{T\phi} \\ \dot{e}_{T\theta} &= \dot{a}_{T\theta} - \dot{\widehat{a}}_{T\theta} \\ &= \dot{a}_{T\theta} - \omega_2 \left(\dot{x}_4 - \dot{z}_2\right) \\ &= \dot{a}_{T\theta} - \omega_2 \big((A_2 + B_2(a_{M\theta} - a_{T\theta}) \end{aligned} \tag{32}$$

$$-A_2 - B_2(a_{M\theta} - \widehat{a}_{T\theta}))$$

$$= \dot{a}_{T\theta} + \omega_2 B_2(a_{T\theta} - \widehat{a}_{T\theta})$$

$$= \dot{a}_{T\theta} + \omega_2 B_2 e_{T\theta} \tag{33}$$

According to Assumption 4.1 and Lemma 3.4, $\lim_{t\to\infty} e_{T\phi} = 0$ and $\lim_{t\to\infty} e_{T\theta} = 0$ are obtained. Thus the predicted target accelerations, $\widehat{a}_{T\theta}$ and $\widehat{a}_{T\phi}$, will converge to the actual target accelerations asymptotically. ∎

4.2. Composite guidance law based on nonlinear disturbance observer

Assumption 4.2: $e_{T\theta}$ and $e_{T\phi}$, which are the disturbance prediction errors, are bounded. Let $\Delta := [\Delta_1; \Delta_2]$ and also Δ_1 and Δ_2 are two positive constants such that

$$\begin{aligned} |e_{T\theta}(t)| = |a_{T\theta} - \hat{a}_{T\theta}| \le \Delta_1 \\ |e_{T\phi}(t)| = |a_{T\phi} - \hat{a}_{T\phi}| \le \Delta_2 \end{aligned} \tag{34}$$

for $t \ge 0$. This assumption emphasizes that the physical systems can produce finite accelerations thereby ensuring their difference to be finite in magnitude.

Composite guidance law consists of the AISM guidance law in (17) and the NDOB technique in (30) and (31).

Theorem 4.2: *Let the chosen guidance system is given by (11)–(12) and let Assumption 4.2 holds true. If the switching gains satisfy $\eta_i > \Delta_i$, $i = 1, 2$, $\dot{\theta}$ and $\dot{\phi}$, which are the LOS angular rates, converge to zero in finite time.*

The proposed composite guidance law is indicated as below.

$$\begin{pmatrix} a_{M\phi} \\ a_{M\theta} \end{pmatrix} = B^{-1} \left(-A - \rho_1 s - \rho_2 \begin{pmatrix} |s_1|^\gamma \, \text{sgn}(s_1) \\ |s_2|^\gamma \, \text{sgn}(s_2) \end{pmatrix} \right.$$

$$\left. - \sum_{j=1}^{2} \left(\begin{vmatrix} c_{1j} \\ c_{2j} \end{vmatrix} \begin{matrix} \text{sgn}(s_1) \\ \text{sgn}(s_2) \end{matrix} \right) \eta_j \hat{\epsilon}_j + \begin{pmatrix} \hat{a}_{T\phi} \\ \hat{a}_{T\theta} \end{pmatrix} \right). \tag{35}$$

Proof: The stability proof is given here similar to those of Theorem 3.2. First, choose the Lyapunov function candidate as $V_3 = \frac{1}{2} s^T s + \frac{1}{2} \sum_{j=1}^{2} \tilde{\epsilon}_j^2$.

Substituting (11)–(12) and (35) into (14) yields the following time derivative of the Lyapunov function:

$$\dot{V}_3 = s^T \dot{s} + \sum_{j=1}^{2} \tilde{\epsilon}_j \dot{\tilde{\epsilon}}_j$$

$$= \left(-\rho_1 s^T s - \rho_2 \sum_{i=1}^{2} |s_i|^{\gamma+1} - \sum_{j=1}^{2} \left(\sum_{i=1}^{2} |c_{ij}||s_i| \right) \eta_j \hat{\epsilon}_j \right)$$

$$+ \left(\sum_{i=1}^{2} c_{i1} s_i \right) a_{T\phi} + \left(\sum_{i=1}^{2} c_{i2} s_i \right) a_{T\theta} - \left(\sum_{i=1}^{2} c_{i1} s_i \right) \widehat{a}_{T\phi}$$

$$- \left(\sum_{i=1}^{2} c_{i2} s_i \right) \widehat{a}_{T\theta} - \sum_{j=1}^{2} \left(\sum_{i=1}^{2} |c_{ij}||s_i| \right) \eta_j \left(\epsilon_j - \widehat{\epsilon}_j \right)$$

$$= \left(-\rho_1 s^T s - \rho_2 \sum_{i=1}^{2} |s_i|^{\gamma+1} - \sum_{j=1}^{2} \left(\sum_{i=1}^{2} |c_{ij}||s_i| \right) \eta_j \epsilon_j \right) + \sum_{j=1}^{2} \left(\sum_{i=1}^{2} |c_{ij}||s_i| \right) \begin{pmatrix} a_{T\phi} - \widehat{a}_{T\phi} \\ a_{T\theta} - \widehat{a}_{T\theta} \end{pmatrix}$$

$$\leqslant -\rho_1 s^T s - \rho_2 \sum_{i=1}^{2} |s_i|^{\gamma+1} - \sum_{j=1}^{2} \left(\sum_{i=1}^{2} |c_{ij}||s_i| \right) \eta_j \epsilon_j + \sum_{j=1}^{2} \left(\sum_{i=1}^{2} |c_{ij}||s_i| \right) \Delta$$

$$\leqslant -\rho_1 s^T s - \rho_2 \sum_{i=1}^{2} |s_i|^{\gamma+1} - \sum_{j=1}^{2} \left(\sum_{i=1}^{2} |c_{ij}||s_i| \right) (\eta_j \epsilon_j - \Delta)$$

$$\leqslant 0 \qquad (36)$$

It can be seen that $\dot{V}_3 \leqslant 0$. Thus $V_3(t) \leqslant V_3(0)$ and $V_3(t)$ is bounded. Therefore, s and $\tilde{\epsilon}_j (j = 1, 2)$ are bounded.

At this stage, we will choose a new Lyapunov function to show that the sliding variables converge to zero in finite time and this function is $V_4 = \frac{1}{2} s^T s$.

The derivative of this Lyapunov function is satisfied as follows:

$$\dot{V}_4 = s^T \dot{s}$$

$$= \left(-\rho_1 s^T s - \rho_2 \sum_{i=1}^{2} |s_i|^{\gamma+1} - \sum_{j=1}^{2} \left(\sum_{i=1}^{2} |c_{ij}||s_i| \right) \eta_j \widehat{\epsilon}_j \right)$$

$$+ \left(\sum_{i=1}^{2} c_{i1} s_i \right) a_{T\phi} + \left(\sum_{i=1}^{2} c_{i2} s_i \right) a_{T\theta} - \left(\sum_{i=1}^{2} c_{i1} s_i \right) \widehat{a}_{T\phi} - \left(\sum_{i=1}^{2} c_{i2} s_i \right) \widehat{a}_{T\theta}$$

$$= \left(-\rho_1 s^T s - \rho_2 \sum_{i=1}^{2} |s_i|^{\gamma+1} - \sum_{j=1}^{2} \left(\sum_{i=1}^{2} |c_{ij}||s_i| \right) \eta_j \widehat{\epsilon}_j \right) + \sum_{j=1}^{2} \left(\sum_{i=1}^{2} |c_{ij}||s_i| \right) \begin{pmatrix} a_{T\phi} - \widehat{a}_{T\phi} \\ a_{T\theta} - \widehat{a}_{T\theta} \end{pmatrix}$$

$$\leqslant -\rho_1 s^T s - \rho_2 \sum_{i=1}^{2} |s_i|^{\gamma+1} - \sum_{j=1}^{2} \left(\sum_{i=1}^{2} |c_{ij}||s_i| \right) \eta_j \widehat{\epsilon}_j + \sum_{j=1}^{2} \left(\sum_{i=1}^{2} |c_{ij}||s_i| \right) \Delta$$

$$\leqslant -\rho_1 s^T s - \rho_2 \sum_{i=1}^{2} |s_i|^{\gamma+1} - \sum_{j=1}^{2} \left(\sum_{i=1}^{2} |c_{ij}||s_i| \right) (\eta_j \widehat{\epsilon}_j - \Delta) \qquad (37)$$

where $\eta_i > \Delta_i$, it can be obtained that

$$\dot{V}_4 \leqslant -\rho_1 s^T s - \rho_2 \sum_{i=1}^{2} |s_i|^{\gamma+1} \qquad (38)$$

Based on Lemma 3.1, we can be rewritten as

$$\dot{V}_4 \leqslant -2\rho_1 V_4 - 2^{\frac{\gamma+1}{2}} \rho_2 V_4^{\frac{\gamma+1}{2}} \qquad (39)$$

According to Lemma 3.2, the sliding variables converges to zero in finite time. Since the remaining steps of the proof are similar to those in Theorem 3.1, they are not shown again

here. Thus, in the light of all this, it is obtained that the LOS angular rates $\dot{\theta}$ and $\dot{\phi}$ converge to zero in finite time, respectively. ∎

In conclusion, the novel composite guidance law is proposed in three-dimensional engagement geometry. Compared to Theorems 3.1, 4.2 has $\hat{a}_{T\theta}$ and $\hat{a}_{T\phi}$ obtained using the NDOB technique and these are given in the guidance system as the feedforward compensation term. This composite guidance law is proposed to improve performance of missile-target interception and to obtain robust results while the chattering is diminished.

5. Numerical simulations

This section demonstrates the results of the numerical simulation for missile-target interception in the 3D geometry. The APNG law and the AISMG law have been chosen to compare whether the proposed composite guidance law is effective (Gürsoy-Demir and Efe 2019). Mathematically the APNG law can be stated as

$$a_{M\phi} = N_1 V_c \dot{\phi} + 0.5 N_2 a_{T\phi} \tag{40}$$

$$a_{M\theta} = N_1 V_c \dot{\theta} + 0.5 N_2 a_{T\theta} \tag{41}$$

where V_c is the closing velocity and N_1, N_2 are positive constants. The AISM guidance law is given in (17), Zhang, Li, and Luo (2013a) and Song and Song (2016).

5.1. Simulation scenarios setting

The initial conditions of the guidance system are chosen as follows. The initial velocity of the missile is $V_{M0} = 800$ m/s and the initial position of the missile is $x_{M0} = 0$ m, $y_{M0} = 5000$ m and $z_{M0} = 0$ m. The initial velocity of the target is $V_{M0} = 400$ m/s and the initial position of the target is $x_{M0} = 1100$ m, $y_{M0} = 5000$ m and $z_{M0} = 0$ m. In addition to these, the initial flight-path angle of the missile is $\phi_{M0} = 0°$ and the heading angle of the missile is $\theta_{M0} = 8°$. For the target, initial flight-path angle is $\phi_{T0} = 10°$ and the heading angle is $\theta_{T0} = 5°$. $g = 9.8$ m/s^2 is used as the gravitational constant (Zhang et al. 2016).

In order to optimize the control parameters used in the presented guidance laws and to obtain high performance, the trial and error method was used. The parameters of the AISM guidance law (17) and the proposed composite guidance law (35) are chosen as $a_1 = b_1 = 0.005$, $a_2 = b_2 = 0.02$, $\alpha_1 = \beta_1 = 0.33$, $\alpha_2 = \beta_2 = 0.5$, $\rho_1 = 0.05$, $\rho_2 = 0.01$. Moreover, the parameters of NDOB (30) and (31) are selected as $\omega_1 = 3000$ and $\omega_2 = -3000$.

Table 1 gives three different cases that take account of target accelerations, and these cases will be used to demonstrate the effectiveness of the presented guidance laws. Additionally, the simulations are carried out under the presence of external disturbances to assess the performance of the guidance law fairly.

Table 1. Accelerations setting of target in interception scenarios.

Interception scenarios	Azimuth acceleration	Elevation acceleration
Non-maneuvering	0	0
Constant maneuvering	$4g$	$4g$
Time-varying maneuvering	$3g + \sin 2\pi t$	$3g + \sin 4\pi t$

5.2. Simulation results

Case 1: Non-maneuvering target

According to the assumption in Case 1, the target has a non-maneuvering motion and the missile aims to intercept this target. For Case 1, the final miss distance and the time

Table 2. Miss distance and interception time for all cases.

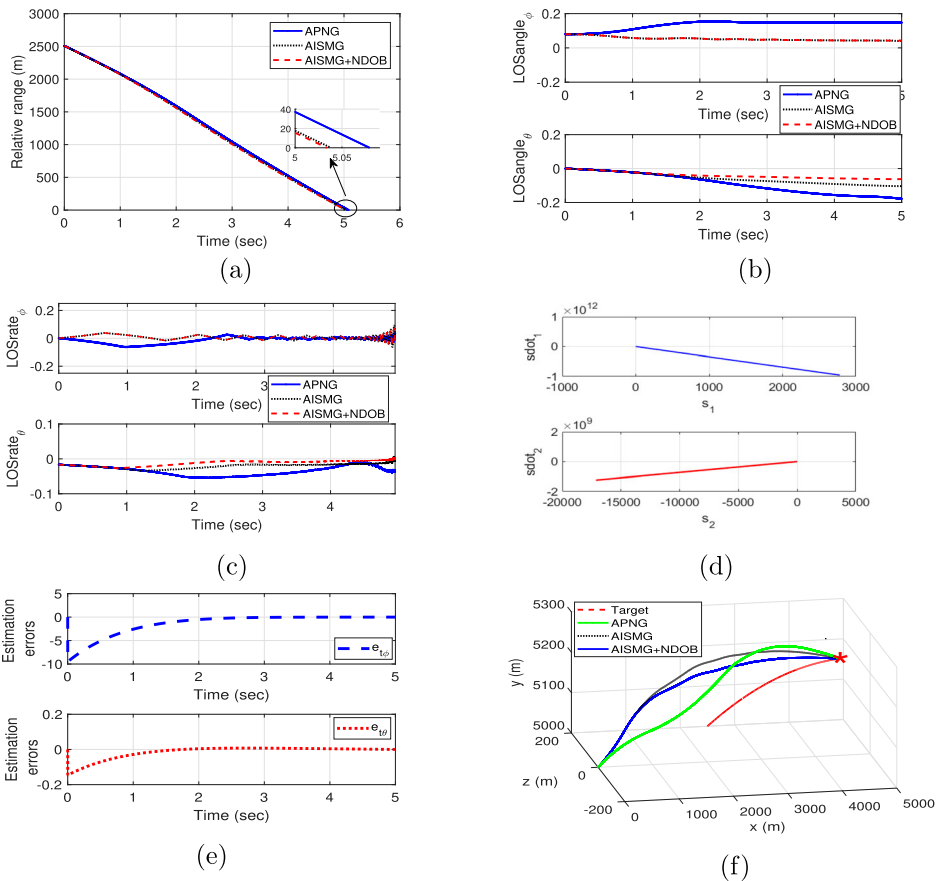| Scenario	Guidance law	Miss distance (m)	Interception time (s)
Case 1	APNGL	0.1918	5.080
	AISMGL	0.1704	5.039
	NDOB-based AISMGL	0.0114	5.035
Case 2	APNGL	0.1915	4.978
	AISMGL	0.2175	4.896
	NDOB-based AISMGL	0.0986	4.865
Case 3	APNGL	0.1487	4.977
	AISMGL	0.2116	4.975
	NDOB-based AISMGL	0.0759	4.927

Figure 2. Results of Case 1 under the APN guidance law, the AISM guidance law and the NDOB-based AISM guidance law: (a) Relative range; (b) LOS angles; (c) LOS rates; (d) Phase space behavior; (e) Target acceleration estimation errors for $a_{T\phi}$ and $a_{T\theta}$; (f) Missile and target trajectories.

of interception are given in Table 2. The relative distance r, the response of LOS angle θ and ϕ, the response of LOS angular rates $\dot{\theta}$ and $\dot{\phi}$, phase space behavior, target acceleration estimation errors for $a_{T\phi}$ and $a_{T\theta}$, missile and target trajectories are demonstrated in Figure 2(a–f), respectively.

Case 2: Constant maneuvering target

According to the assumption in this case, the target has a constant maneuver motion and the missile aims to intercept this target. For Case 2, the final miss distance and the time of interception are presented in Table 2. The relative distance r, the response of LOS angle θ and ϕ, the response of LOS angular rates $\dot{\theta}$ and $\dot{\phi}$, phase space behavior, target acceleration estimation errors for $a_{T\phi}$ and $a_{T\theta}$, missile and target trajectories are demonstrated in Figure 3(a–f), respectively.

Case 3: Time-varying maneuvering target

According to the assumption in Case 3, the target has a time-varying maneuvering movement, which is different from the second case, in which case the missile intercepts
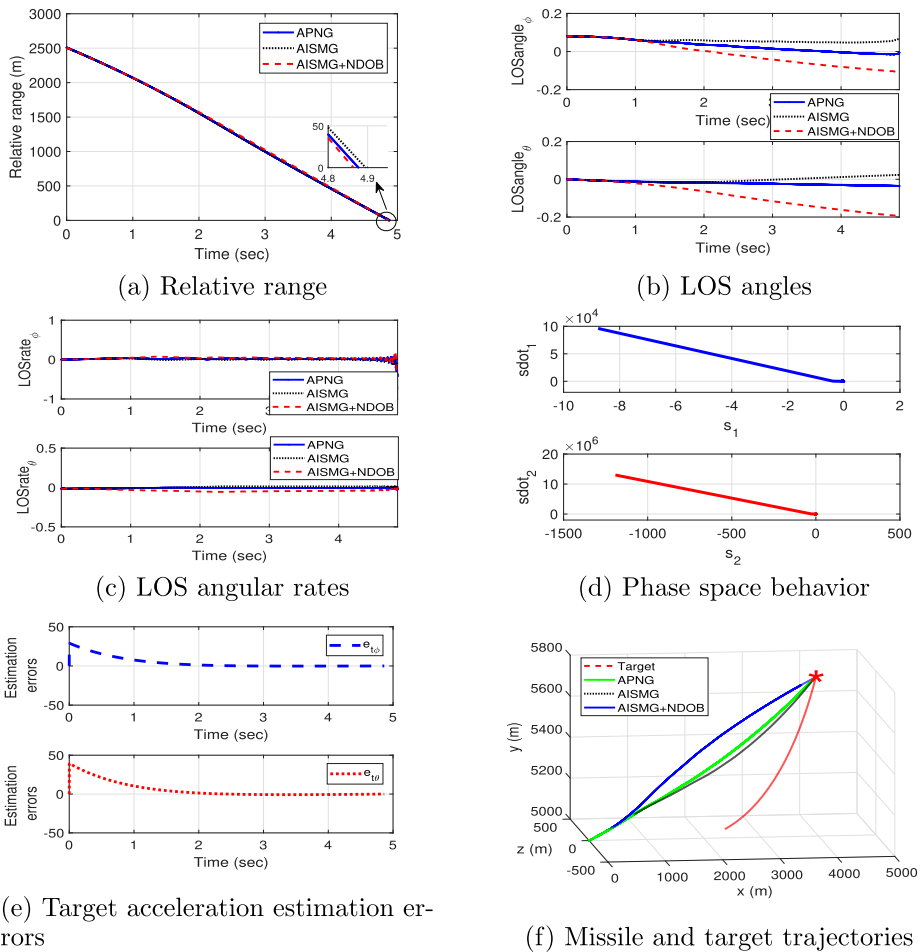

(a) Relative range

(b) LOS angles

(c) LOS angular rates

(d) Phase space behavior

(e) Target acceleration estimation errors

(f) Missile and target trajectories

Figure 3. Results of Case 2 under the APN guidance law, the AISM guidance law and the NDOB-based AISM guidance law : (a) relative range; (b) LOS angles; (c) LOS rates; (d) switching variables; (e) the actual and estimated target acceleration $a_{T\theta}$; (f) the actual and estimated target acceleration $a_{T\phi}$.

this target. For Case 3, the final miss distance and the time of interception are given in Table 2. The relative distance r, the response of LOS angle θ and ϕ, the response of LOS angular rates $\dot{\theta}$ and $\dot{\phi}$, phase space behavior, target acceleration estimation errors for $a_{T\phi}$ and $a_{T\theta}$, missile and target trajectories are demonstrated in Figure 4(a–f), respectively.

It can be seen from Figures 2(a) to 4(a) that the relative range decreases to zero at intercept time in all of the guidance laws. It can be understood from here that these guidance laws can guarantee to intercept the target successfully. However, the APN guidance law and the AISM guidance law approach zero over a longer period of time than the NDOB-based AISM guidance law, resulting in additional cost in terms of convergence time. Figures 2(b)–4(b) show the response of the LOS angles. Figures 2(c)–4(c) show the response of LOS angular rates. It has also been reported that the LOS angular rates come close to
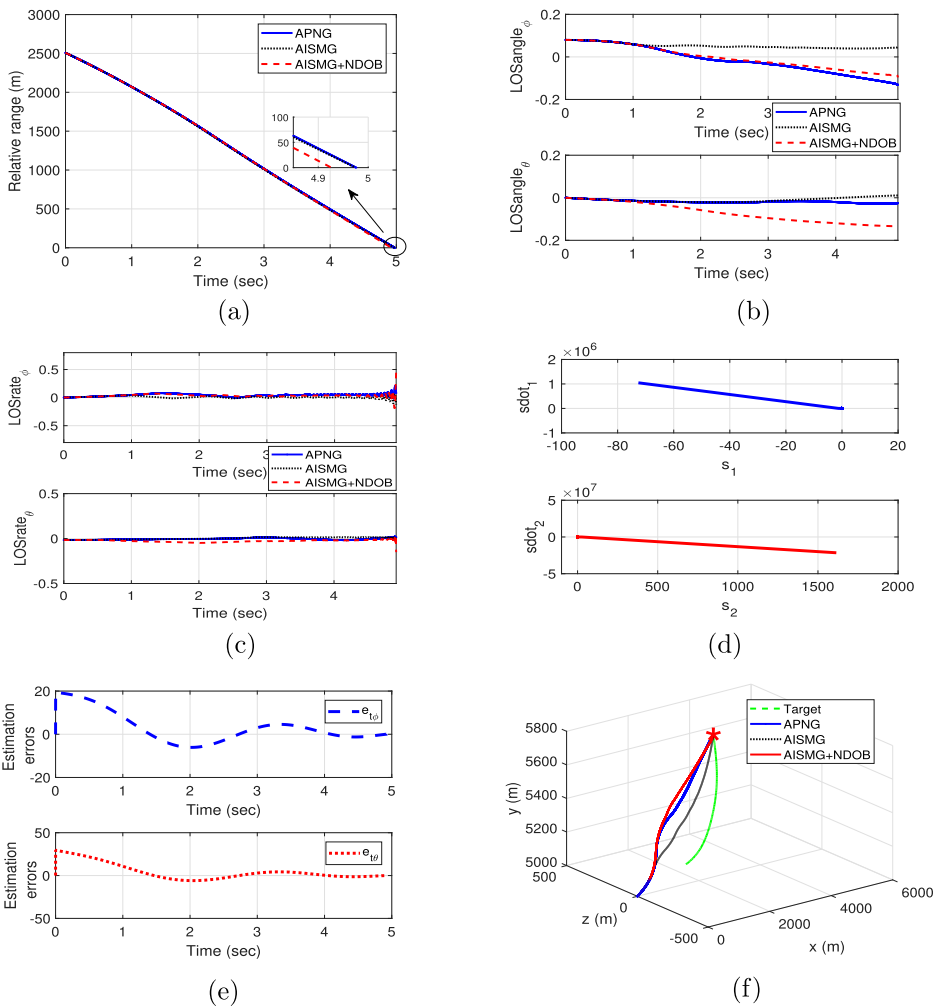

Figure 4. Results of Case 3 under the APN guidance law, the AISM guidance law and the NDOB-based AISM guidance law: (a) relative range; (b) LOS angles; (c) LOS rates; (d) phase space behavior; (e) target acceleration estimation errors for $a_{T\phi}$ and $a_{T\theta}$; (f) missile and target trajectories.

zero for all of the guidance laws in cases where the missile is intercepting the target that has a non-maneuvering movement. Figures 2(d)–4(d) illustrate the controlled phase space behavior of the switching manifold defined for the elevation angle and the azimuth angle for the proposed guidance law. Figures 2(e) and 4(e) demonstrate the disturbance estimation errors obtained using the NDOB technique. The estimated accelerations by the NDOB converge to the real target's accelerations and so the estimation errors finally reach zero. As are demonstrated in Figures 2(e) and 4(e), the presented all guidance laws can intercept the target successfully. Also, with the proposed guidance law, it can be observed that the missile has shorter trajectories.

The miss distance and the time of interception for all presented cases are tabulated in Table 2. As can be seen from the table, the presented guidance laws guarantee the miss distance being below 0.25 m in the three cases considered. This means that the missile successfully intercepts the targets by the hit-to-kill strategy (Shtessel, Shkolnikov, and Levant 2009). The results have shown that the proposed novel guidance law outperforms the classical APNG law and the AISMG law and it leads to display less interception time and less miss distance compared to other. Besides, when the missile intercepts the target which has large maneuverability, the performance of the proposed guidance law observed to be even better.

6. Conclusion

In this paper, a novel three-dimensional composite guidance law by using the adaptive integral sliding mode control method and the nonlinear disturbance observer technique is presented for missile guidance systems. At the outset, an ISM guidance law is presented for eliminating the reaching phase of the traditional SMC method. Then, the AISM guidance law is designed for the case in which the target accelerations profile's upper bound is unavailable. The results have shown that the reaching phase is eliminated and a robust guidance law is obtained without the need for an upper bound information of the target accelerations. Additionally, it is analytically demonstrated in our study that the LOS angular rates converge to zero in finite time, as expected from a guidance law. The nonlinear disturbance observer technique has been utilized to generate an estimate by considering the target accelerations as disturbances. The estimated accelerations of the target are provided to the system as a compensation term. Thus the chattering phenomenon that is one of the disadvantages of SMC is eliminated by using the proposed composite guidance law. Simulations on the missile guidance system proved the effectiveness and the feasibility of the proposed guidance law compared to its alternatives.

Acknowledgments

Disclosure statement

Funding

Notes on contributors

Handan Gürsoy Demir received the B.Sc. degree in Computer Engineering from Cukurova University, Adana, Turkey, in 2012, and the M.Sc. degree in Computer Engineering from Hacettepe University, Ankara, Turkey, in 2016. She is currently working toward the Ph.D. degree in Computer Engineering at Hacettepe University, Ankara, Turkey.
Her research interests include nonlinear, robust and adaptive control with applications to missile systems.

Mehmet Önder Efe received the B.Sc. degree in Electronics and Communications Engineering from Istanbul Technical University, Istanbul, Turkey, in 1993, the M.Sc. degree in Systems and Control Engineering from Boğaziçi University, Istanbul, Turkey, in 1996, and the Ph.D. degree in Electrical and Electronics Engineering from Boğaziçi University, in 2000.
He is currently a professor with the Department of Computer Engineering, Hacettepe University, Ankara, Turkey.
Dr. Efe serves and served as an associate editor of the *IEEE Transactions on Industrial Electronics*, *IEEE Transactions on Industrial Informatics*, *IEEE/ASME Transactions on Mechatronics*, and Editor of *Transactions of the Institute of Measurement and Control and Measurement and Control*.

ORCID

Handan Gürsoy-Demir http://orcid.org/0000-0001-5486-454X
Mehmet Önder Efe http://orcid.org/0000-0002-5992-895X

References

Bhat, Sanjay P., and Dennis S. Bernstein. 2005. "Geometric Homogeneity with Applications to Finite-Time Stability." *Mathematics of Control, Signals and Systems* 17 (2): 101–127.

Chen, Syuan-Yi, Hsin-Han Chiang, Tung-Sheng Liu, and Chih-Hung Chang. 2019. "Precision Motion Control of Permanent Magnet Linear Synchronous Motors Using Adaptive Fuzzy Fractional-Order Sliding-Mode Control." *IEEE/ASME Transactions on Mechatronics* 24 (2): 741–752.

Chen, Bei, Tinggang Jia, and Yugang Niu. 2016. "Robust Fuzzy Control for Stochastic Markovian Jumping Systems Via Sliding Mode Method." *International Journal of General Systems* 45 (5): 604–618.

Dhananjay, Narayanachar, Kai-Yew Lum, and Jian-Xin Xu. 2012. "Proportional Navigation with Delayed Line-of-Sight Rate." *IEEE Transactions on Control Systems Technology* 21 (1): 247–253.

Golestani, Mehdi, Iman Mohammadzaman, Mohammad Javad Yazdanpanah, and Ahmad Reza Vali. 2015. "Application of Finite-Time Integral Sliding Mode to Guidance Law Design." *ASME Journal of Dynamic Systems Measurement and Control* 137 (11): 114501.

Guo, Jianguo, Yifei Li, and Jun Zhou. 2019. "A New Continuous Adaptive Finite Time Guidance Law Against Highly Maneuvering Targets." *Aerospace Science and Technology* 85: 40–47.

Gürsoy-Demir, Handan, and Mehmet Önder Efe. 2019. "Comparison of Three-Dimensional Guidance Laws For Missile Guidance System." In *10th Ankara International Aerospace Conference*. Ankara, Turkey: Metu.

Harl, Nathan, and S. N. Balakrishnan. 2011. "Impact Time and Angle Guidance with Sliding Mode Control." *IEEE Transactions on Control Systems Technology* 20 (6): 1436–1449.

Hou, Zhiwei, Lei Liu, Yongji Wang, Jian Huang, and Huijin Fan. 2016. "Terminal Impact Angle Constraint Guidance with Dual Sliding Surfaces and Model-Free Target Acceleration Estimator." *IEEE Transactions on Control Systems Technology* 25 (1): 85–100.

Hu, Qinglei, Tuo Han, and Ming Xin. 2019. "Three-Dimensional Guidance for Various Target Motions with Terminal Angle Constraints Using Twisting Control." *IEEE Transactions on Industrial Electronics (1982)* 67 (2): 1242–1253.

Jia, Huaiyuan, Weiwei Shang, Fei Xie, Bin Zhang, and Shuang Cong. 2019. "Second-Order Sliding-Mode-Based Synchronization Control of Cable-Driven Parallel Robots." *IEEE/ASME Transactions on Mechatronics* 25 (1): 383–394.

Khalil, Hassan K. 2002. *Nonlinear Systems*. Upper Saddle River.

Li, X. B., G. R. Zhao, S. Liu, and X. Han. 2019. "Adaptive Integral Sliding Mode Guidance Law with Impact Angle Constraint Considering Autopilot Lag." In *Journal of Physics: Conference Series*, Vol. 1267, 012081. Xi'an, China: IOP Publishing.

Liang, Yew-Wen, Chih-Chiang Chen, Der-Cherng Liaw, Yang-Ching Feng, Chiz-Chung Cheng, and Chun-Hone Chen. 2014. "Robust Guidance Law Via Integral-Sliding-Mode Scheme." *Journal of Guidance, Control, and Dynamics* 37 (3): 1038–1042.

Man, Chaoyuan, Rongjie Liu, and Shihua Li. 2019. "Three-dimensional Suboptimal Guidance Law Based on $\theta-D$ Technique and Nonlinear Disturbance Observer." *Proceedings of the Institution of Mechanical Engineers, Part G: Journal of Aerospace Engineering* 233 (14): 5122–5133.

Mehmet Önder, Efe. 2011. "Integral Sliding Mode Control of a Quadrotor with Fractional Order Reaching Dynamics." *Transactions of the Institute of Measurement and Control* 33 (8): 985–1003.

Meng, Kezi, and Di Zhou. 2018. "Super-Twisting Integral-Sliding-Mode Guidance Law Considering Autopilot Dynamics." *Proceedings of the Institution of Mechanical Engineers, Part G: Journal of Aerospace Engineering* 232 (9): 1787–1799.

Murtaugh, Stephen A., and Harry E. Criel. 1966. "Fundamentals of Proportional Navigation." *IEEE Spectrum* 3 (12): 75–85.

Nair, Ranjith Ravindranathan, Laxmidhar Behera, and Swagat Kumar. 2017. "Event-Triggered Finite-Time Integral Sliding Mode Controller for Consensus-Based Formation of Multirobot Systems with Disturbances." *IEEE Transactions on Control Systems Technology* 27 (1): 39–47.

Ohishi, Kiyoshi. 1983. "Torque-Speed Regulation of DC Motor Based on Load Torque Estimation." In *IEEJ International Power Electronics Conference, IPEC-TOKYO*, Vol. 2, 1209–1216. Tokyo, Japan: The Institute of Electrical Engineers of Japan.

Sariyildiz, Emre, Roberto Oboe, and Kouhei Ohnishi. 2019. "Disturbance Observer-Based Robust Control and Its Applications: 35th Anniversary Overview." *IEEE Transactions on Industrial Electronics (1982)* 67 (3): 2042–2053.

Shtessel, Yuri B., Ilya A. Shkolnikov, and Arie Levant. 2009. "Guidance and Control of Missile Interceptor Using Second-Order Sliding Modes." *IEEE Transactions on Aerospace and Electronic Systems* 45 (1): 110–124.

Si, Yu-Jie, and Shen-Min Song. 2019. "Continuous Reaching Law Based Three-Dimensional Finite-Time Guidance Law Against Maneuvering Targets." *Transactions of the Institute of Measurement and Control* 41 (2): 321–339.

Song, Junhong, and Shenmin Song. 2016. "Three-Dimensional Guidance Law Based on Adaptive Integral Sliding Mode Control." *Chinese Journal of Aeronautics* 29 (1): 202–214.

Song, Junhong, Shenmin Song, and Huibo Zhou. 2016. "Adaptive Nonsingular Fast Terminal Sliding Mode Guidance Law with Impact Angle Constraints." *International Journal of Control, Automation, and Systems* 14 (1): 99–114.

Utkin, Vadim. 1977. "Variable Structure Systems with Sliding Modes." *IEEE Transactions on Automatic Control* 22 (2): 212–222.

Utkin, Vadim, Jürgen Guldner, and Jingxin Shi. 2009. *Sliding Mode Control in Electro-Mechanical Systems*. CRC Press.

Utkin, Vadim, and Jingxin Shi. 1996. "Integral Sliding Mode in Systems Operating Under Uncertainty Conditions." In *Proceedings of 35th IEEE Conference on Decision and Control*, Vol. 4, 4591–4596. Kobe, Japan: IEEE.

Wang, Jiang, and Shaoming He. 2016. "Optimal Integral Sliding Mode Guidance Law Based on Generalized Model Predictive Control." *Proceedings of the Institution of Mechanical Engineers, Part I: Journal of Systems and Control Engineering* 230 (7): 610–621.

Wang, Jianmei, Xiaoyuan Luo, Li Wang, Zhiqiang Zuo, and Xinping Guan. 2019. "Integral Sliding Mode Control Using a Disturbance Observer for Vehicle Platoons." *IEEE Transactions on Industrial Electronics (1982)* 67 (8): 6639–6648.

Wang, Shubo, Liang Tao, Qiang Chen, Jing Na, and Xuemei Ren. 2020. "USDE-Based Sliding Mode Control for Servo Mechanisms With Unknown System Dynamics." *IEEE/ASME Transactions on Mechatronics* 25 (2): 1056–1066.

Yaghi, Murad, and Mehmet Onder Efe. 2020. "$\mathcal{H}_2/\mathcal{H}_\infty$-Neural-Based FOPID Controller Applied for Radar-Guided Missile." *IEEE Transactions on Industrial Electronics* 67 (6): 4806–4814.

Yu, Shuanghe, Xinghuo Yu, Bijan Shirinzadeh, and Zhihong Man. 2005. "Continuous Finite-Time Control for Robotic Manipulators with Terminal Sliding Mode." *Automatica* 41 (11): 1957–1964.

Zhang, Zhenxing, Shihua Li, and Sheng Luo. 2013a. "Composite Guidance Laws Based on Sliding Mode Control with Impact Angle Constraint and Autopilot Lag." *Transactions of the Institute of Measurement and Control* 35 (6): 764–776.

Zhang, Zhenxing, Shihua Li, and Sheng Luo. 2013b. "Terminal Guidance Laws of Missile Based on ISMC and NDOB with Impact Angle Constraint." *Aerospace Science and Technology* 31 (1): 30–41.

Zhang, Xiaojian, Mingyong Liu, Yang Li, and Feihu Zhang. 2019. "Impact Angle Control Based on Integral Sliding Mode Manifold and Extended State Observer." *Proceedings of the Institution of Mechanical Engineers, Part G: Journal of Aerospace Engineering* 233 (6): 2131–2140.

Zhang, Zhenxing, Chaoyuan Man, Shihua Li, and Shi Jin. 2016. "Finite-Time Guidance Laws for Three-Dimensional Missile-Target Interception." *Proceedings of the Institution of Mechanical Engineers, Part G: Journal of Aerospace Engineering* 230 (2): 392–403.